SI Appendix

Structural basis for ligand binding to an enzyme by a conformational selection pathway

Michael Kovermann[a,b]*, Christin Grundström[a], A. Elisabeth Sauer-Eriksson[a], Uwe H. Sauer[a], & Magnus Wolf-Watz[a]*

[a] Department of Chemistry, Umeå University, SE-901 87 Umeå, Sweden

[b] Department of Chemistry, University of Konstanz, Universitätsstrasse 10, D-78457 Konstanz, Germany

*Correspondence to:

michael.kovermann@uni-konstanz.de

magnus.wolf-watz@umu.se

Experimental procedures

Protein production and crystallization. AdK G56C, AdK T163C, and AdK^{cc} were synthezised and sequenced by Genscript (USA). Sample preparation: Wild type and singly mutated AdK variants were produced as described previously for wild type AdK (1). AdK^{cc} was overexpressed in BL21(DE3) cells from plasmids controlled by the AdK promotor. Cells were harvested by centrifugation and resuspended in lysis buffer containing 50 mM Tris, pH 7.5 and 2 mM dithiothreitol (DTT). After a freeze-thaw cycle, the cells were lysed by sonication, centrifuged to remove cell debris, and the protein was purified from the supernatant by binding to Blue Sepharose followed by elution using buffers providing a linear NaCl gradient from 0 to 0.5 M NaCl and containing 2 mM DTT. Pooled fractions containing AdK^{cc} were subjected to size-exclusion chromatography in a buffer consisting of 30 mM 3-(N-morpholino)propanesulfonic acid (MOPS) and 50 mM NaCl (note no DTT was present at this stage) at pH 7.0. Fractions containing AdK^{cc} were pooled and diluted to 2 μM in the size-exclusion chromatography buffer. Disulfide bond crosslinking was performed by incubating the 2 μM AdK^{cc} solution for 20 hours at 37°C. The monomeric protein fraction was collected and stored at -20 °C at a concentration of 300 μM. All concentrations of AdK^{cc} were determined using an extinction coefficient of 10430 $M^{-1}cm^{-1}$ at λ = 280 nm. Ap5a concentrations were determined using an extinction coefficient of 30000 $M^{-1}cm^{-1}$ and concentrations of both AMP and ATP using an extinction coefficient of 15400 $M^{-1}cm^{-1}$, at λ = 260 nm in each case. ^{15}N- and $^{15}N/^{13}C$-labeled protein was produced using defined media and supplementation of ^{15}N and or ^{13}C-glucose as previously described (1).

The $AdK^{cc,ox}$ protein was crystallized as described previously (2). Briefly, the purified $AdK^{cc,ox}$ was dialyzed against 50 mM NaCl and 30 mM 2-(*N*-morpholino)ethanesulfonic acid (MES) buffer (pH 6.0) and concentrated to 13 $mg \cdot ml^{-1}$ using an Amicon ultracentrifugation filter device

(Millipore; 3 kDa molecular weight cutoff) and co-crystallized at 18°C with a 5 M excess of P1,P5-di(adenosine-5′)pentaphosphate (Ap5a) using the vapor-diffusion hanging drop method. A drop containing 1 μL of protein solution was mixed with 1 μL of precipitant and equilibrated against 1 mL of precipitant solution containing a range of 26–28% PEG 8K, 10 mM $CoCl_2$, and 0.1 M sodium acetate at pH 5.8. Crystals grew to dimensions of 0.1 × 0.05 × 0.4 mm^3 after 5 days.

Data collection, phasing, and refinement. Crystals were taken directly from the growth drop and vitrified in a N_2 gas stream maintained at 100 K using a Cryostream Cooler (Oxford Cryosystems), tested for diffraction, and subsequently stored in liquid nitrogen. High-resolution synchrotron diffraction data were collected at the Max II laboratory (Lund, Sweden) at beam line I911-2 using X-ray radiation of λ = 1.038 Å at 100 K. Data were processed and scaled using XDS (3) followed by Pointless, and Aimless from the CCP4 suite (4). Data-collection statistics are listed in Table 1. Crystals of $AdK^{cc,ox}$ belong to space group $P2_122_1$ and contain two protein molecules in the asymmetric unit. The phases for structure determination were obtained by molecular replacement using the program PHASER from the PHENIX suite (5) and the AdK-Ap5a complex (1AKE (2)) as the search model. The structures were built and refined using the programs COOT (6) and PHENIX REFINE. The electron density map was well defined except for one surface-exposed loop connecting residues Glu75 to Asn79. The final model has no Ramachandran plot outliers and the clash score was 1. The atomic coordinates and structure factors were assigned PDB code 5EJE and were deposited in the Protein Data Bank, Research Collaboratory for Structural Bioinformatics, Rutgers University, New Brunswick, NJ (http://www.rcsb.org/). Structural superimposition was carried out in COOT using SSM (7).

Kinetic assay for probing enzyme activity. Enzyme kinetic parameters for ATP turnover in the direction of ADP formation were quantified for wild type AdK, $AdK^{cc,ox}$, $AdK^{cc,red}$, AdK G56C, and AdK G163C at 25°C using a coupled spectroscopic ATPase assay (8), as follows: ATP was added, at various concentrations, with 10 μL of protein solution to buffer containing 100 mM Tris, 80 mM KCl, 0.2 mM NADH, 0.4 mM phosphoenolpyruvate, 0.3 mM AMP, and 2 mM $MgCl_2$ (pH 7.5), to a final volume of 471 μL. Changes in absorption at 340 nm with time were monitored (in a Varian Cary 50 UV-visible spectrophotometer) to obtain the reaction velocity, v, which was plotted against ATP concentration, c_{ATP}. Maximal turnover rate (k_{cat}) and ATP affinity (K_M) under the experimental conditions were then calculated from the Michaelis–Menten relation:

$$v = (k_{cat} * c_{ATP})/(K_M + c_{ATP})$$

Isothermal titration calorimetry. Isothermal calorimetry experiments were carried out at 25°C using a MicroCal Auto-iTC200 instrument (GE Healthcare). Isothermal titration reference cell was filled with sample buffer (30 mM MOPS, 50 mM NaCl, pH 7.0), and protein solutions (380 μL) were placed in the sample cell then titrated with either AMP, ATP or Ap5a loaded in the syringe (100 μL). The instrumental settings were: reference power 4 $\mu cal \cdot s^{-1}$, initial delay 200 s, stirring speed 400 rpm, spacing 150 s, filter 5 s, injection 0.3 μL (first injection) or 1.5 μL (subsequent injections), and low-feedback mode.

The $AdK^{cc,ox}$ and AMP concentrations were 50 and 400 μM, respectively, in one experiment, and 40 and 250 μM, respectively, in a second experiment. AMP to $AdK^{cc,red}$, ATP to $AdK^{cc,ox}$, ATP to $AdK^{cc,red}$, Ap5a to $AdK^{cc,ox}$, Ap5a to $AdK^{cc,red}$ and Ap5a to wild type AdK (while TCEP is present) titrations were performed with corresponding concentrations. Again, the same

concentrations were used for AMP, ATP or Ap5a titration to single mutation variant AdK G56C or AdK T163C.

No change in enthalpy was detected in control experiments (involving injecting AMP, ATP or Ap5a into buffer solution). Raw data were collected, corrected for ligand heats of dilution, and integrated using MicroCal Origin software. Data sets were fitted by using a single-site binding (for AMP and ATP interaction to all AdK variants probed and Ap5a interaction to wild type AdK, AdK G56C and AdK T163C) or a two-site binding model (Ap5a titration to $AdK^{cc,ox}$ and $AdK^{cc,red}$) to yield the dissociation constant, K_D, the apparent enthalpy of binding, ΔH^0, and the stoichiometry of binding, n.

NMR spectroscopy. All NMR experiments were conducted in a Bruker Avance III HD 850 MHz spectrometer equipped with a z-gradient cryogenic probe using 30 mM MOPS and 50 mM NaCl (pH 7.0) and 5% D_2O (v/v) as sample buffer and at T = 298 K. All two-dimensional (2D) and three-dimensional (3D) NMR data sets were processed with NMRPipe (9) and analyzed in NMRView (10). One-dimensional NMR data were processed and analyzed in TopSpin 3.1.

Assignment experiments. Backbone ^{15}N, $^{1}H^{N}$, $^{13}C\alpha$, and ^{13}CO chemical shifts of $AdK^{cc,ox}$ and $AdK^{cc,red}$ were assigned by acquisition of 2D ^{1}H-^{15}N HSQC and 3D HNCA, HNCO and HN(CO)CA experiments (11). Weighted differences in chemical shifts, $\Delta\omega$, were calculated using:

$$\Delta\omega = (((\Delta^{1}H^{N})^2 + (\Delta^{15}N/5)^2)/2)^{0.5}$$

where $\Delta^{1}H^{N}$ is the change in proton and $\Delta^{15}N$ is the change in nitrogen dimension.

Ap5a was added in two times excess relative to wild type AdK, $AdK^{cc,ox}$ and $AdK^{cc,red}$.

Heteronuclear nuclear Overhauser effect (hNOE) experiments. We probed picosecond-to-nanosecond time scale dynamics of wild type AdK, $AdK^{cc,ox}$, and $AdK^{cc,red}$ by *h*NOE experiments as described in (12).

One-dimensional real-time NMR. Reduction of the disulfide in $AdK^{cc,ox}$ with time was monitored by acquiring one-dimensional proton spectra at 5-minute intervals. The most high-field-shifted methyl group was integrated between −0.25 and −0.22 ppm for $AdK^{cc,ox}$ and between −0.29 and −0.26 ppm for $AdK^{cc,red}$. The increase/decrease of the integral, I, was fitted to an exponential function:

$$I = I_0 \exp(kt)$$

where k is the rate constant describing the increase or decrease of the signal intensity of the methyl group under investigation.

RDC measurements. $AdK^{cc,ox}$ was aligned in 10 mg/ml Pf1 phages ordered from PROFOS. The alignment tensor was determined by using MODULE (13) and back calculation of measured RDC data against wild type AdK (4AKE) or Ap5a-bound AdK (1AKE).

Relaxation dispersion. The dispersion of the transversal relaxation rate, $R_{2,\mathrm{eff}}$, was acquired according to (14).

Interaction of transition state mimic Ap5a to AdK

Since the crystallographic analysis clearly shows that $AdK^{cc,ox}$ binds Ap5a it was interesting to probe the interaction also with ITC. In light of potential steric occlusion effects due to the closed nature of $AdK^{cc,ox}$ it was notable to observe tight binding and a high quality thermogram for this interaction (Fig. S10A). The binding is characterized by two distinct binding events with K_D

values of 2.5 and 250 nM, respectively (Table 2). In addition, the interaction occurs with a significantly increased enthalpic contribution compared to the wild type (Fig. S10A and Table 2). The increased enthalpic contribution was found to depend on the presence of the two cysteines in positions 56 and 163 since the enthalpic contribution observed for interaction of Ap5a to both $AdK^{cc,ox}$ and $AdK^{cc,red}$ matches the sum of the corresponding values of the singly mutated variants. Additionally, a comparison between apo and the Ap5a-bound state of both $AdK^{cc,ox}$ and $AdK^{cc,red}$ made on basis of ^{1}H-^{15}N NMR HSQC spectra reveals profound spectral differences underlying the strong ability of Ap5a to interact with AdK^{cc} in both oxidized and reduced states (Fig. S10 B and C). Additional comparisons of the various Ap5a complexes are shown in Fig. S10 D-H. Comparison of Ap5a-bound wild type to apo AdK^{cc} is included and the differences in chemical shifts, in part, depend on substantial changes to the electronic environment from the highly charged Ap5a molecule (Fig. S10 D and E). A comparison among Ap5a bound states shows a large degree of similarity for wild type AdK, $AdK^{cc,ox}$ and $AdK^{cc,red}$ (Fig. S10 F-H).

Figure legends

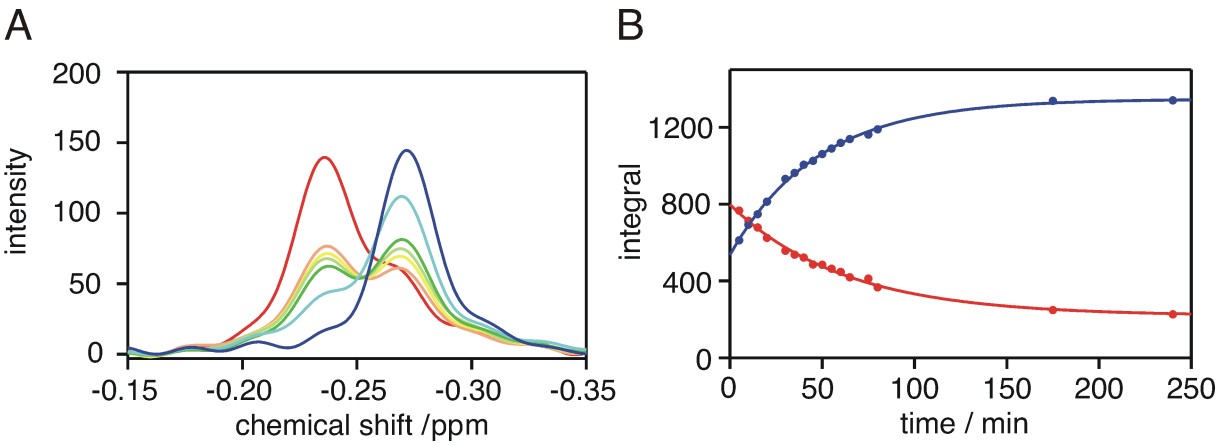

Fig. S1 Real-time NMR observation of TCEP induced $AdK^{cc,ox}$ reduction. (A) Time-dependent change of the chemical environment of an isolated methyl group of $AdK^{cc,ox}$ upon adding TCEP. The color coding corresponds to the absence of TCEP (red), and incubation of $AdK^{cc,ox}$ with TCEP for 5 (orange), 10 (yellow), 15 (light green), 20 (green), 45 (cyan), and 390 minutes (blue). (B) Data for both oxidized (red) and reduced (blue) states presented in (A) were integrated and a mono-exponential function was applied to evaluate the kinetics of $AdK^{cc,ox}$ reduction induced by TCEP. The rate constant for signal decrease was determined to 0.97±0.05 h^{-1}. An independent analysis of the signal increase yielded a rate constant of 1.26±0.03 h^{-1}.

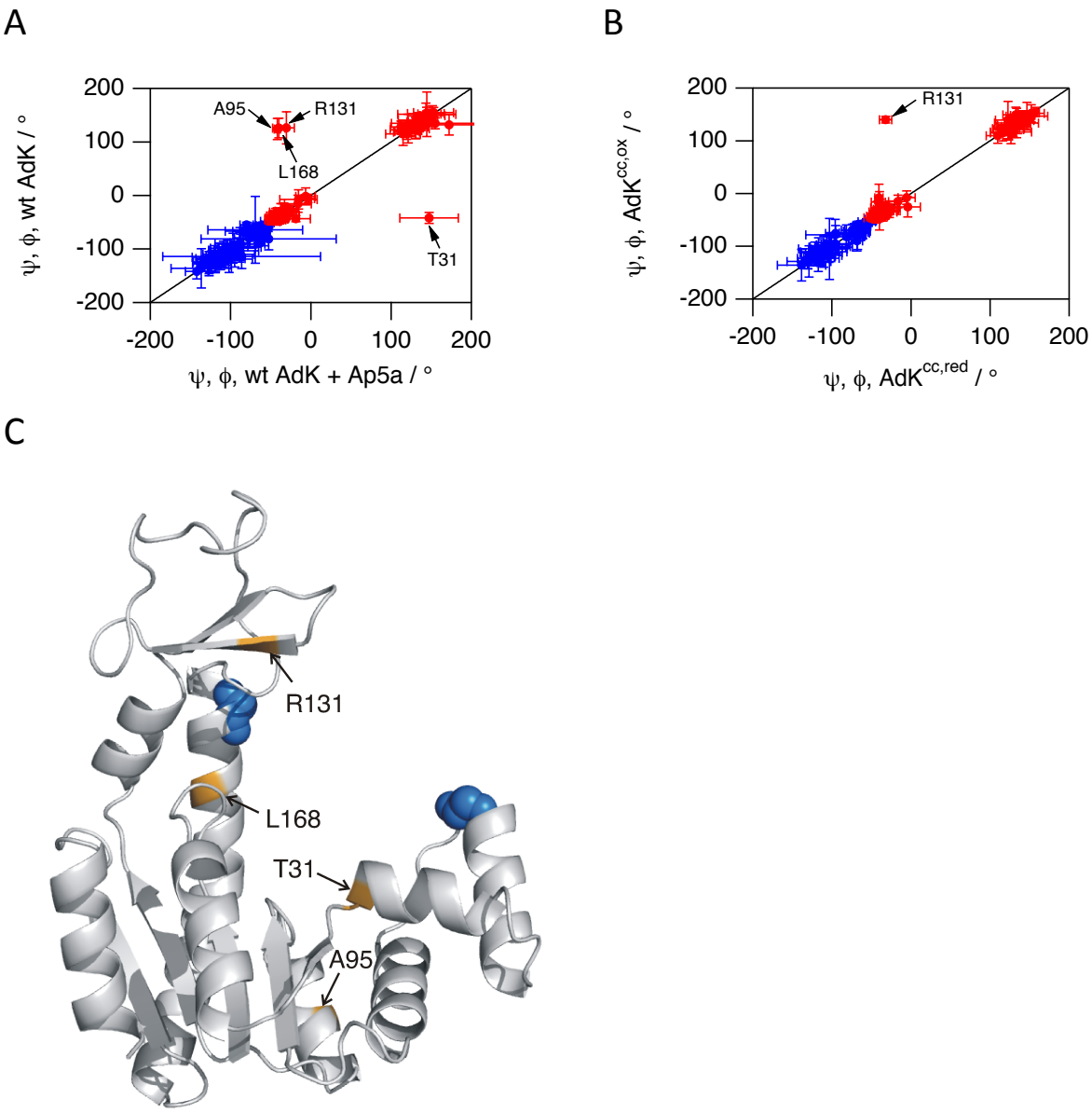

Fig. S2 Analysis of dihedral angles ψ (colored in blue) and ϕ (colored in red) by applying TALOS+. The analysis was performed by comparing apo with Ap5a-bound wild type AdK as shown in (A) and by comparing $AdK^{cc,ox}$ with $AdK^{cc,red}$ as shown in (B). Residues T31, A95, R131 and L168 experience changes in values of ψ, ϕ analyzing wild type AdK or R131 analyzing AdK^{cc} are mapped onto the structure of apo wild type AdK in (C). Residues G56 and T163 which have been used as cystein mutation sites in AdK^{cc} are highlighted in blue.

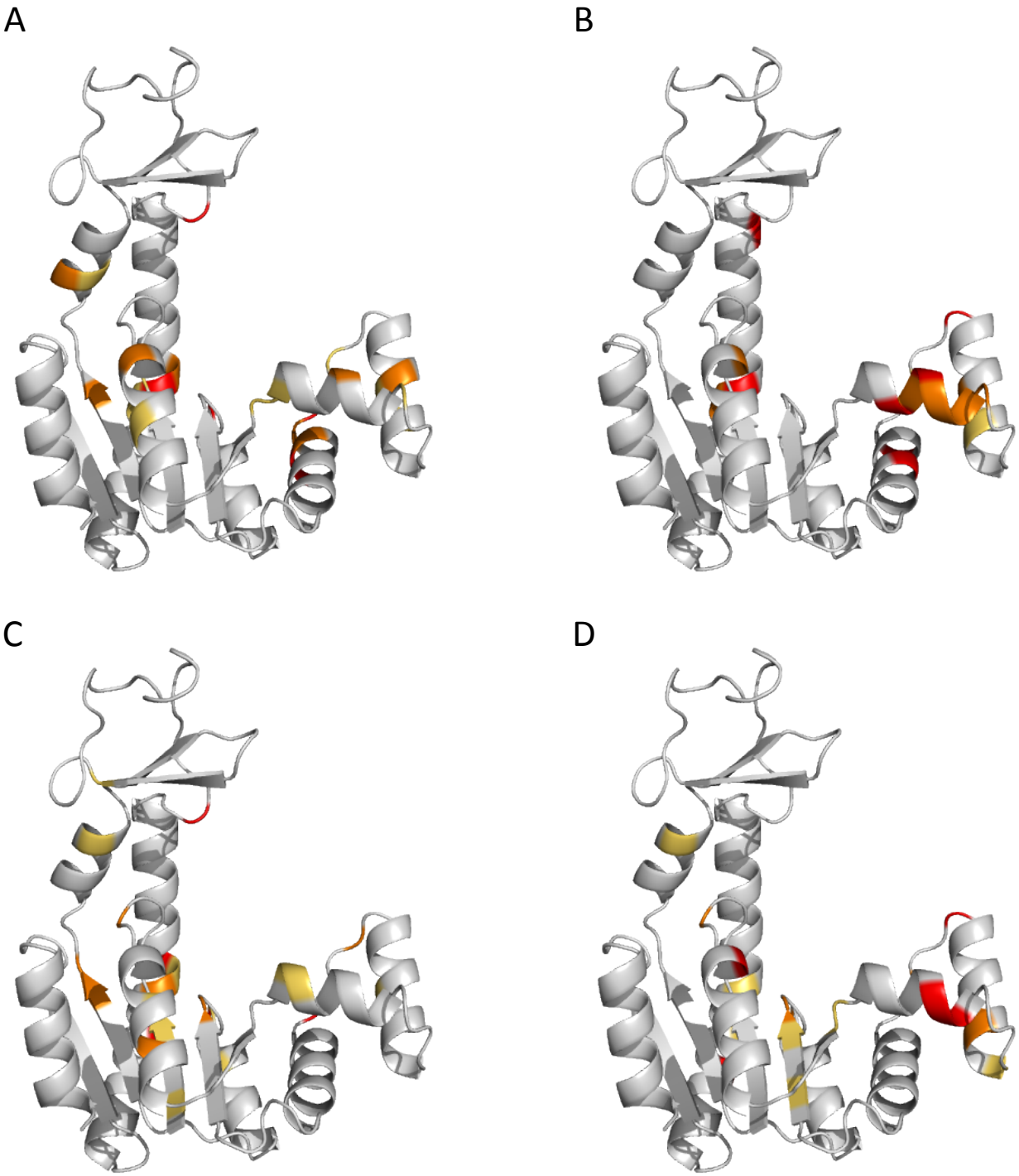

Fig. S3 Mapping of changes to C^{α} (A, B) and CO (C, D) chemical shifts upon addition of Ap5a to wild type AdK (A, C) and addition of TCEP to $AdK^{cc,ox}$ (B, D). The color coding is as follows: (A, B) $\Delta\omega > 2$ ppm, red; $1.3 < \Delta\omega < 2$ ppm, bright orange; $1 < \Delta\omega < 1.3$ ppm, yellow orange. (C)

$\Delta\omega > 1.5$ ppm, red; $1.3 < \Delta\omega < 1.5$ ppm, bright orange; $1 < \Delta\omega < 1.3$ ppm, yellow orange. (D) $\Delta\omega > 0.8$ ppm, red; $0.5 < \Delta\omega < 0.8$ ppm, bright orange; $0.3 < \Delta\omega < 0.5$ ppm, yellow orange.

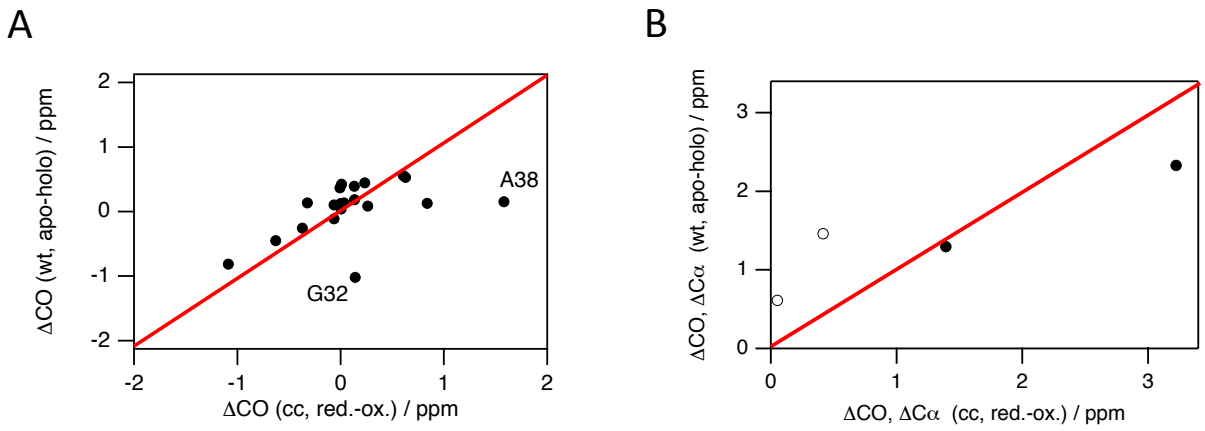

Fig. S4 Correlation of sign sensitive changes of chemical shifts following addition of Ap5a to wild type AdK (y-axis) and addition of TCEP to $AdK^{cc,ox}$ (x-axis). Changes of chemical shifts are shown for CO signals originating from residues in the AMPbd domain (A) and for CO (open circles) and C^{α} signals (closed circles) from T175 and A176 in the central helix (B).

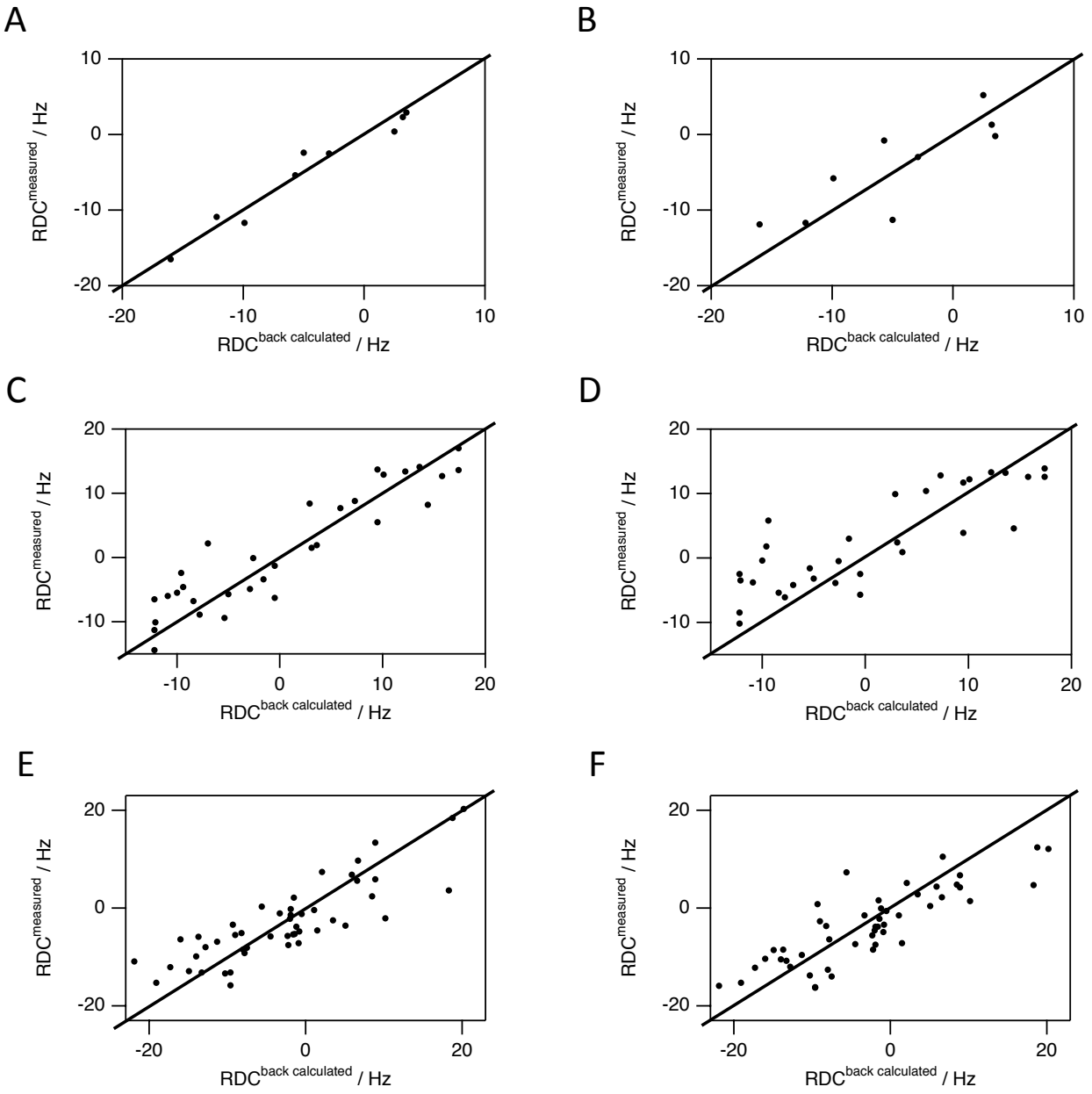

Fig. S5 Analysis of residual dipolar couplings (RDCs) of $AdK^{cc,ox}$ induced by Pf1 phages. The calculation of measured RDC values of $AdK^{cc,ox}$ was done for the AMPbd domain (A, B), the ATPlid domain (C, D) and core domain related residues (E, F) using the open-like apo wild type AdK structure 4AKE.pdb (B, D, F) as well the closed-like Ap5a-bound AdK structure 1AKE.pdb (A, C, E). Back calculation leads to X^2 values as follows: 7.3E01 (A), 4.9E02 (B), 1.9E03 (C), 4.3E03 (D), 5.2E03 (E), and 5.5E03 (F).

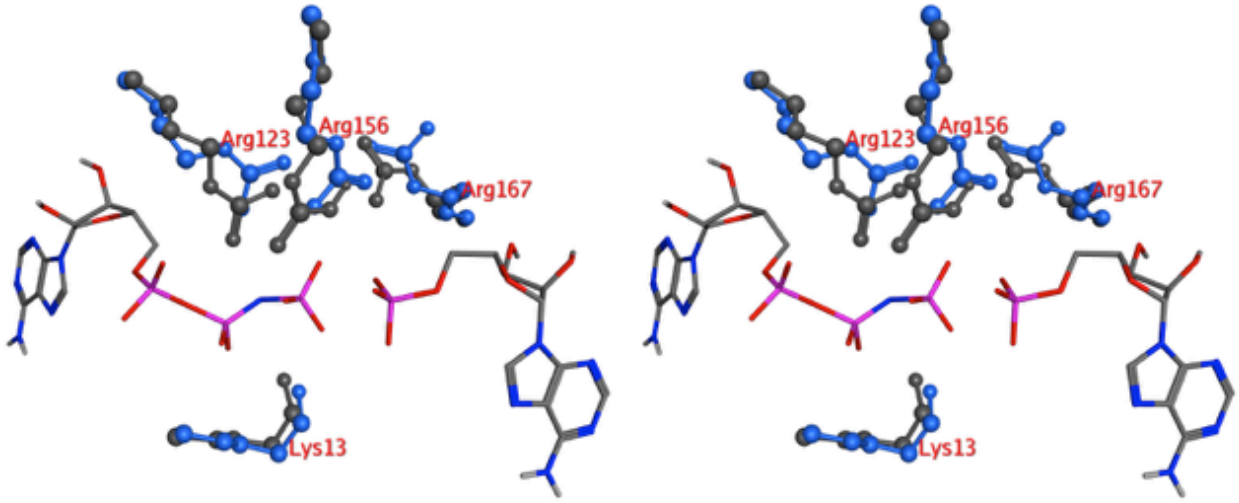

Fig. S6 Catalytic conformation of active site residues in Ap5a bound $AdK^{cc,ox}$. The conformations of catalytically crucial residues Lys13, Arg123, Arg156 and Arg167 are shown in stereo for AdK in complex with AMPPNP and AMP (gray, 1ANK.pdb) and for $AdK^{cc,ox}$ in complex with the transition state mimic Ap5a (blue). Shown are the AMPPNP (left) and AMP (right) molecules in 1ANK.pdb. The complex between AMPPNP and AMP represents a catalytically competent state that is arrested as a result of the slowly hydrolyzing nature of AMPPNP. The protein complexes were superposed on C^{α} atoms for residues 1-214 which resulted in an rmsd of 0.56 Å.

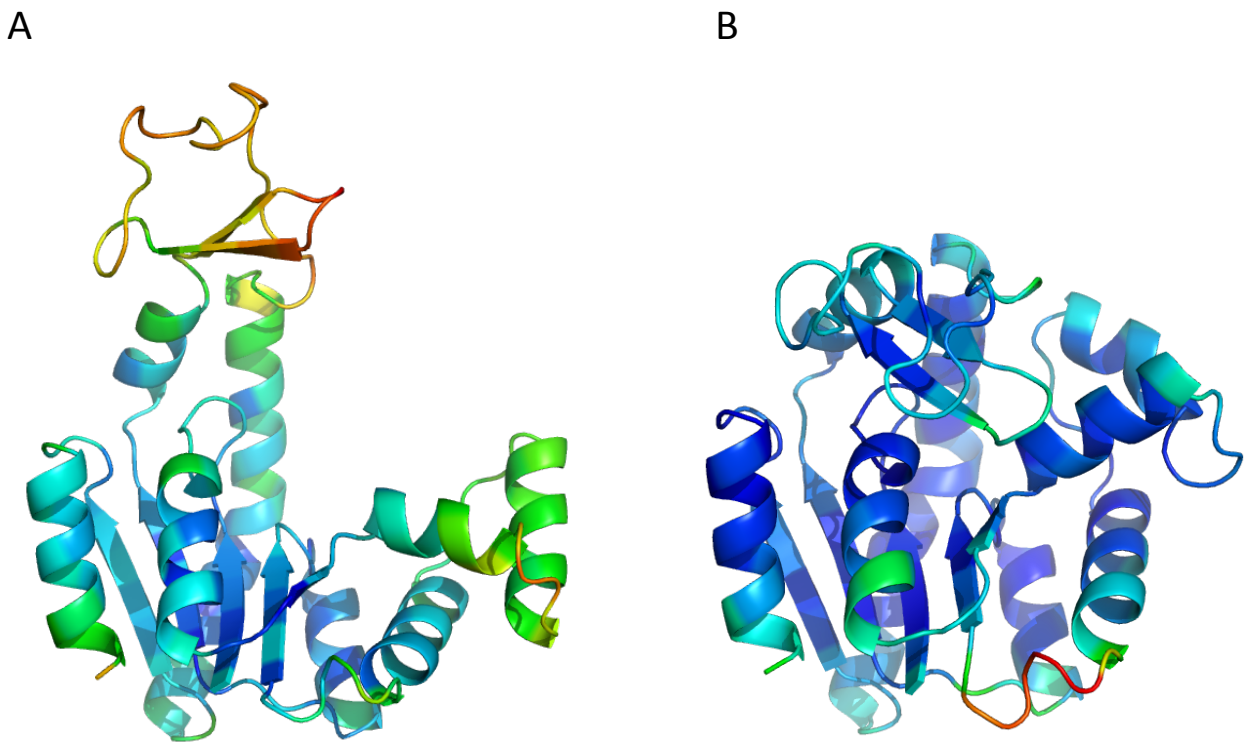

Fig. S7 *B* factor analysis of crystallographic structures of apo wild type AdK (4AKE.pdb) (A) and Ap5a-bound $AdK^{cc,ox}$ (5EJE.pdb) (B). The color coding refers to a rainbow scale by presenting large values of *B* factors in red whereas low values are shown in blue.

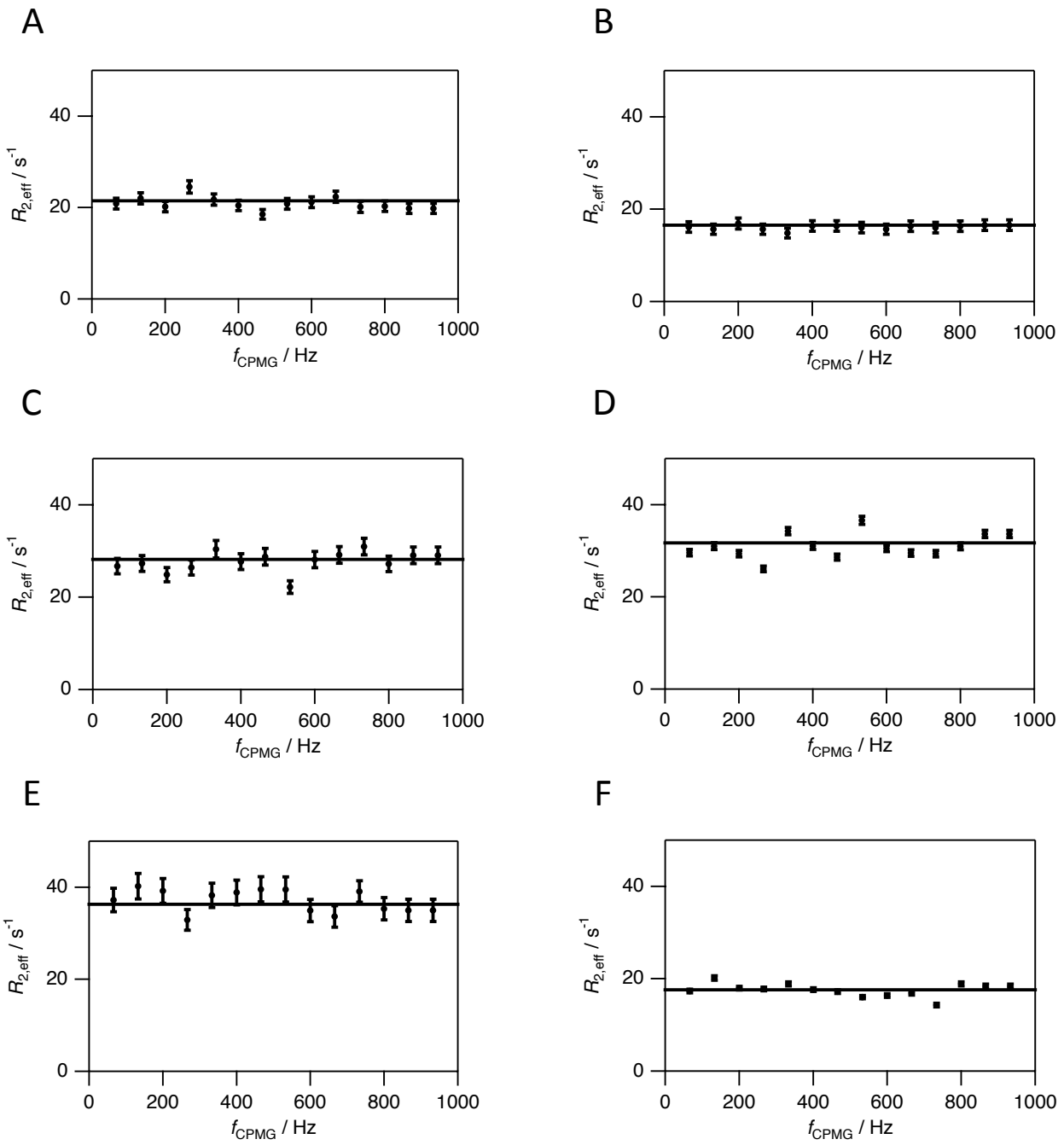

Fig. S8 Profiles of ^{15}N dispersion experiments for the transversal relaxation rate acquired for AdK^{cc,ox} (44). The profiles shown comprise residues in the AMPbd: L35 (A), C56 (B), Q74 (C) as well as residues belonging to the ATPlid: S129 (D), C163 (E) and V164 (F). The residues with engineered cysteines in AdK^{cc} are underlined.

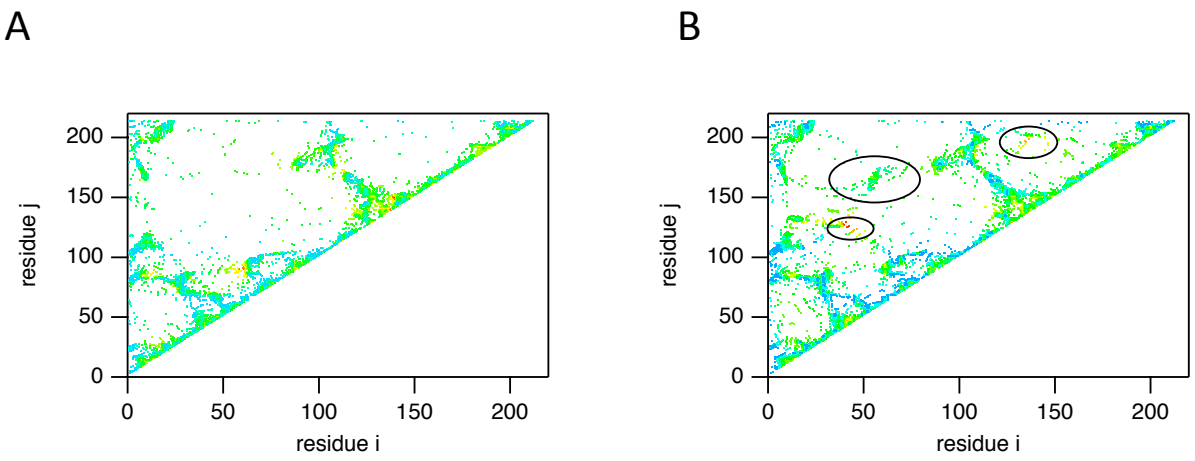

Fig. S9 Local mutational frustration index (14) for open-like wild type AdK (A) (4AKE.pdb) and closed-like Ap5a-bound wild type AdK (B) (1AKE.pdb). Analysis of 1AKE.pdb reveals three additional interresidual contributions to the local mutational frustration index compared to 4AKE.pdb. These differences are marked by ellipses colored in black. Note that C56 and C163 were used as sites for disulfide bridging of AdK in this study. The color coding of the local mutational frustration index is as follows: -2, red (highly frustrated); -1.5, orange; -1, yellow green; -0.5, green; +0.5, dark green; +1, cyan; +1.5, light blue (minimally frustrated).

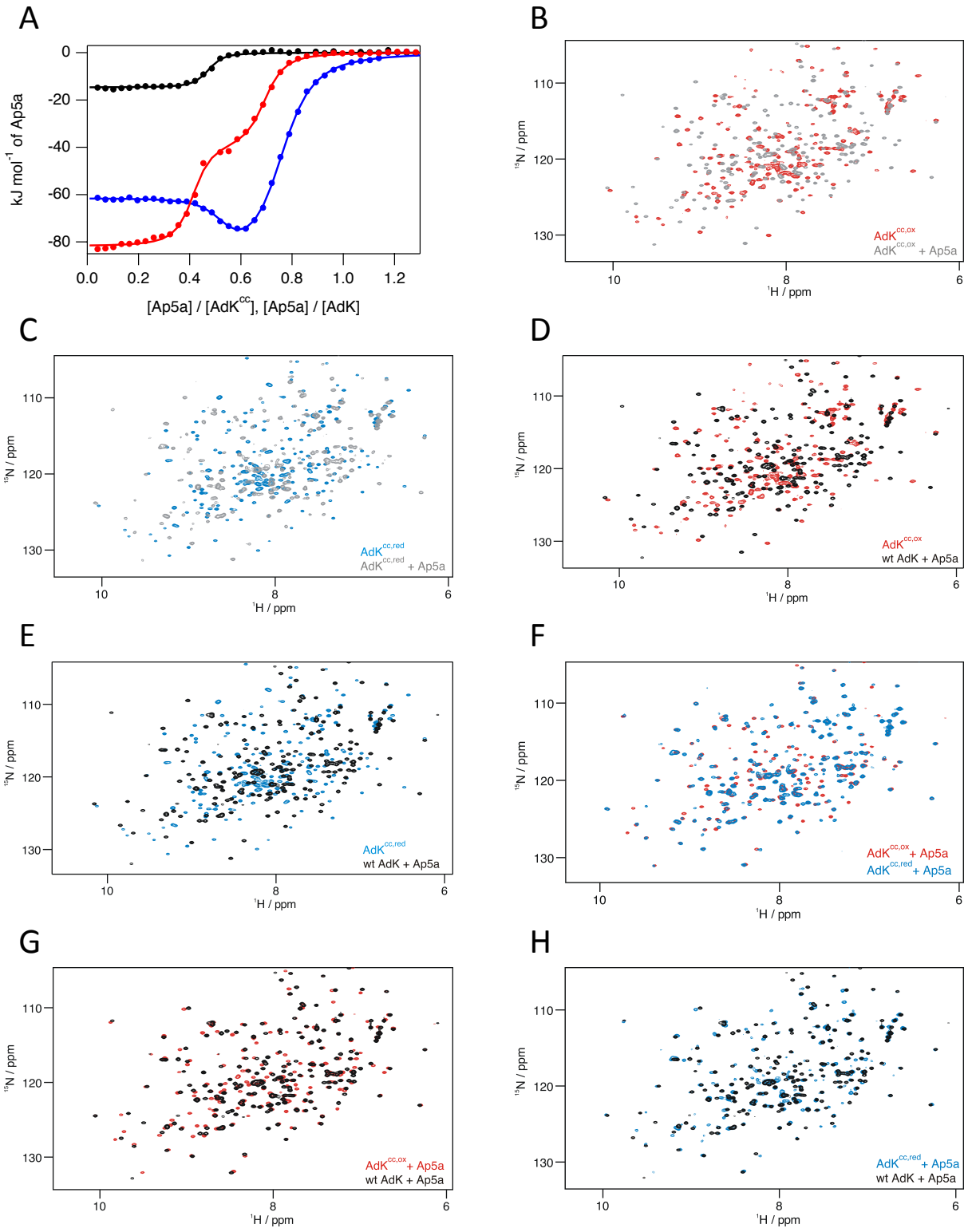

Fig. S10 Interaction of the transition state mimic Ap5a to AdK. (A) Individual ITC profiles were obtained at $T = 298$ K by adding Ap5a to $AdK^{cc,ox}$ under oxidative conditions (colored in red), for

adding Ap5a to $AdK^{cc,red}$ under reducing conditions (colored in blue) as well as for adding Ap5a to wild type AdK (colored in black). Corresponding thermodynamic parameters are listed in Table 2. (B) – (H) ^{1}H-^{15}N HSQC NMR spectra of complexes between different AdK variants and Ap5a. Ap5a has been added to $AdK^{cc,ox}$ (apo state colored in red whereas Ap5a-bound state is shown in gray) as presented in (B) and to $AdK^{cc,red}$ (apo state colored in blue whereas Ap5a-bound state is shown in gray) as presented in (C). A spectral overlay between apo $AdK^{cc,ox}$ (colored in red) and Ap5a-bound wild type AdK (colored in black) is shown in (D) whereas (E) presents an overlay between apo $AdK^{cc,red}$ (colored in blue) and Ap5a-bound wild type AdK (colored in black). Ap5a-bound $AdK^{cc,ox}$ (colored in red) is compared with Ap5a-bound $AdK^{cc,red}$ (colored in blue) in (F) whereas a comparison between the Ap5a-bound states of $AdK^{cc,ox}$ (colored in red) and wild type AdK (colored in black) as of $AdK^{cc,red}$ (colored in blue) and wild type AdK (colored in black) is shown in (G) and (H), respectively.

Table S1

Changes of ^{1}H-^{15}N chemical shifts (ppm) induced by reducing $AdK^{cc,ox}$ to $AdK^{cc,red}$ using TCEP. aa: amino acid

aa	$\Delta^{1}H$-^{15}N	aa	$\Delta^{1}H$-^{15}N	aa	$\Delta^{1}H$-^{15}N	aa	$\Delta^{1}H$-^{15}N
2	0.02	84	0.09	134	0.01	189	0.01
3	0.04	85	0.12	135	0.02	190	0.01
4	0.07	86	0.17	136	0.02	191	0.03
6	0.03	88	0.12	137	0.05	192	0.02
7	0.03	89	0.21	138	0.02	193	0.04
8	0.00	90	0.05	141	0.00	194	0.01
11	0.05	92	0.05	142	0.01	195	0.06
14	0.22	93	0.03	143	0.00	196	0.07
18	0.10	94	0.10	144	0.01	197	0.03
19	0.16	95	0.05	145	0.03	198	0.03
20	0.11	97	0.09	146	0.00	199	0.04
21	0.04	98	0.08	147	0.00	200	0.02
22	0.05	99	0.08	148	0.01	202	0.02
24	0.10	100	0.07	149	0.01	203	0.03
25	0.06	101	0.05	150	0.00	204	0.03
26	0.03	102	0.04	151	0.01	205	0.02
28	0.02	103	0.02	152	0.00	206	0.03
29	0.26	105	0.08	153	0.00	207	0.01
30	0.33	106	0.01	154	0.02	208	0.05
32	0.12	107	0.02	155	0.04	209	0.01
34	0.08	108	0.04	156	0.04	210	0.02
35	0.16	109	0.07	157	0.10	211	0.00
37	0.05	110	0.05	159	0.18	212	0.01
38	0.10	111	0.15	160	0.05	213	0.01
43	0.12	113	0.02	161	0.03	214	0.06
44	0.14	114	0.03	162	0.09		
46	0.07	115	0.01	163	0.05		
48	0.05	116	0.02	164	0.21		
56	0.09	117	0.03	165	0.10		
61	0.02	118	0.05	166	0.12		
62	0.38	119	0.09	175	0.10		
66	0.10	120	0.01	176	0.13		
73	0.00	121	0.08	178	0.19		
74	0.04	123	0.05	179	0.02		
75	0.03	124	0.01	180	0.10		
76	0.01	125	0.02	181	0.04		
77	0.03	126	0.00	182	0.02		
78	0.04	127	0.00	183	0.01		
79	0.12	129	0.00	184	0.07		
80	0.12	130	0.00	185	0.07		
81	0.05	131	0.00	186	0.02		
82	0.05	132	0.01	187	0.05		
83	0.03	133	0.03	188	0.01		

Table S2

Changes of ^{1}H-^{15}N chemical shifts (ppm) induced by interaction of Ap5a to wild type AdK.
aa: amino acid

aa	$\Delta^{1}H$-^{15}N	aa	$\Delta^{1}H$-^{15}N	aa	$\Delta^{1}H$-^{15}N	aa	$\Delta^{1}H$-^{15}N	aa	$\Delta^{1}H$-^{15}N
2	0.30	62	0.43	114	0.11	161	0.05	213	0.12
3	0.38	63	0.84	115	0.14	162	0.05	214	0.07
5	0.70	64	0.72	116	0.20	163	0.11		
6	0.40	65	0.38	117	0.25	164	0.22		
7	0.71	66	0.53	118	0.06	165	0.42		
8	0.30	68	0.73	119	0.35	166	0.19		
16	0.44	69	0.10	120	0.31	170	0.03		
17	0.83	70	0.16	121	0.41	171	0.10		
18	0.37	71	0.58	122	0.28	172	0.31		
19	0.23	72	0.16	123	0.19	174	0.73		
22	0.31	73	0.22	124	0.56	175	0.53		
23	0.28	74	0.07	125	0.21	176	0.46		
24	0.35	75	0.06	126	0.18	178	1.26		
25	0.30	76	0.06	127	0.08	179	0.37		
26	0.35	77	0.06	129	0.03	180	0.23		
28	0.35	78	0.10	130	0.08	181	0.27		
29	0.73	79	0.36	131	0.04	182	0.30		
30	0.37	80	0.28	132	0.16	183	0.36		
32	0.88	81	0.12	133	0.15	184	0.19		
33	0.41	82	0.14	134	0.20	185	0.44		
35	0.19	83	0.12	135	0.21	186	0.05		
36	0.64	84	0.07	136	0.02	188	0.02		
40	0.24	88	0.37	137	0.69	189	0.05		
41	0.15	89	0.06	138	0.47	190	0.07		
42	0.08	90	0.58	141	0.04	191	0.07		
43	0.23	92	0.16	142	0.02	194	0.27		
44	0.13	93	0.21	143	0.00	195	0.09		
45	0.24	94	0.29	144	0.08	196	0.12		
46	0.25	95	0.16	145	0.02	197	0.09		
47	0.19	97	0.04	146	0.01	198	0.02		
48	0.23	98	0.15	147	0.04	199	0.09		
50	0.41	99	0.21	148	0.04	200	0.18		
51	0.34	100	0.18	149	0.03	202	0.18		
52	0.20	101	0.10	150	0.01	203	0.18		
53	0.17	102	0.20	151	0.02	204	0.07		
54	0.60	103	0.33	152	0.03	205	0.11		
55	0.11	105	0.11	153	0.05	206	0.13		
56	0.24	106	0.18	154	0.10	207	0.02		
57	0.32	107	0.27	155	0.33	208	0.12		
58	0.78	109	0.34	156	0.07	209	0.13		
59	0.36	110	0.47	158	0.30	210	0.14		
60	0.31	111	0.20	159	0.80	211	0.19		
61	0.60	113	0.38	160	0.06	212	0.20		

Table S3

Changes of C^{α} and CO chemical shifts (ppm) induced by reducing of $AdK^{cc,ox}$ to $AdK^{cc,red}$ using TCEP. aa: amino acid

aa	ΔC^{α}	ΔCO	aa	ΔC^{α}	ΔCO	aa	ΔC^{α}	ΔCO	aa	ΔC^{α}	ΔCO	aa	ΔC^{α}	ΔCO
1	0.26		61	0.02	0.01	114	0.02	0.01	159	0.02	0.04	212	0.02	0.03
2	0.93	0.24	62	3.10	0.26	115	0.04	0.02	160	0.10	0.13	213	0.04	0.01
3	0.06	0.23	66	0.20	0.06	116	0.64	0.01	161	0.01	0.02	214	0.04	0.03
4	0.41	0.04	67	5.06		117	0.00	0.12	162	0.12	0.24	204	0.02	0.05
5	0.20		73	0.09	0.01	118	0.01	0.02	163	4.31	0.18	205	0.01	0.01
6	0.06	0.16	74	0.11	0.00	119	0.30	0.36	164	0.02		206	0.07	0.11
7	0.64	0.19	75	0.14	0.13	120	0.09	0.02	165	0.17	0.28	207	0.02	0.10
8	0.09	0.07	76	0.00	0.03	121	0.12	0.20	175	3.22	0.42	208	0.00	0.02
11	0.15	0.67	77	0.17	0.13	122	0.12		176	1.39	0.05	209	0.12	0.10
13	0.27		78	0.03	0.00	123	0.01	0.12	177	0.26		210	0.00	0.04
14	1.34	1.72	79	0.03	0.23	124	0.01	0.01	178	0.05	0.36	211	0.03	0.09
15	0.04		80	0.06	0.05	125	0.00	0.01	179	0.26	0.14	212	0.02	0.03
18	0.01	0.05	81	0.14	0.35	126	0.04	0.02	180	0.05	0.04	213	0.04	0.01
19	0.07	0.03	82	0.01	0.03	127	0.05	0.02	181	0.15	0.83	214	0.04	0.03
20	0.01	0.09	83	0.29	0.45	128	0.06		182	0.18	0.09			
21	0.14	0.02	84	0.00	0.56	129	0.02	0.01	183	0.01	0.03			
22	0.02	0.01	85	0.48	0.23	130	0.06	0.02	184	0.13	0.03			
24	0.21	0.04	86	0.64	0.20	131	0.00	0.01	185	0.04	0.01			
25	0.03	0.03	87	0.21		132	0.02	0.00	186	0.04	0.02			
26	0.04	0.02	88	0.48	0.11	133	0.03	0.12	187	0.19	0.03			
27	0.12		89	0.10	0.53	134	0.02	0.06	188	0.13	0.02			
28	0.06	0.14	90	0.28	0.23	135	0.05	0.03	189	0.00	0.06			
29	0.05	0.44	91	0.05		136	0.02	0.02	190	0.04	0.03			
30	0.17	0.37	92	0.19	0.12	137	0.15	0.05	191	0.06	0.02			
31	0.71		93	0.03	0.23	138	0.06	0.07	192	0.11	0.02			
32	0.40	0.14	94	0.02	0.14	140	0.08		193	0.12	0.01			
33	0.61		95	0.03	0.00	141	0.02	0.02	194	0.06	0.06			
34	2.23		96	0.16		142	0.01	0.01	195	0.01	0.13			
35	1.45		97	0.02	0.12	143	0.00	0.01	196	0.14	0.07			
36	2.01		98	0.10	0.02	144	0.06	0.00	197	0.01	0.00			
37	1.42	1.09	99	0.02	0.01	145	0.01	0.00	198	0.16	0.15			
38	1.40	1.58	100	0.07	0.20	146	0.07	0.01	199	0.08	0.02			
39	1.45		101	0.07	0.09	147	0.05	0.00	200	0.02	0.02			
40	1.88		102	0.02	0.03	148	0.04	0.01	201	0.14				
43	0.78	0.06	103	0.01	0.03	149	0.10	0.01	202	0.13	0.01			
44	2.05	0.32	105	0.01	0.04	150	0.11	0.00	203	0.00	0.05			
45	0.84		106	0.02	0.05	151	0.01	0.00	204	0.02	0.05			
46	1.19	0.61	107	0.05	0.03	152	0.02	0.06	205	0.01	0.01			
47	0.25		108	0.01	0.02	153	0.00	0.02	206	0.07	0.11			
48	0.29	0.63	109	0.21	0.01	154	0.00	0.04	207	0.02	0.10			
49	1.54		110	0.34	0.23	155	0.01	0.02	208	0.00	0.02			
56	2.29	0.84	111	0.02	0.13	156	0.01	0.00	209	0.12	0.10			
57	0.87		112	0.07		157	0.13	0.00	210	0.00	0.04			
59	1.07	0.63	113	0.00	0.07	158	0.19		211	0.03	0.09			

Table S4

Changes of C^{α} and CO chemical shifts (ppm) induced by interaction of Ap5a to wild type AdK. aa: amino acid

aa	ΔC^{α}	ΔCO	aa	ΔC^{α}	ΔCO	aa	ΔC^{α}	ΔCO	aa	ΔC^{α}	ΔCO	aa	ΔC^{α}	ΔCO
2	0.40	1.07	49	1.18	1.02	95	0.04	0.08	140	0.18	0.00	184	0.21	0.06
3	0.06	0.33	50	1.47	0.54	96	0.48	0.00	141	0.14	0.02	185	0.16	0.02
4	0.34	0.22	51	0.11	0.28	97	0.18	0.30	142	0.05	0.00	186	0.27	0.09
5	0.14	1.11	52	0.68	0.82	98	0.11	0.10	143	0.12	0.09	187	0.00	0.05
6	0.34	0.10	53	0.27	0.15	99	0.14	0.01	144	0.06	0.05	188	0.05	0.07
7	1.22	0.39	54	0.14	0.36	100	0.39	0.16	145	0.07	0.03	189	0.05	0.02
8	0.71	0.54	55	0.03	0.78	101	0.12	0.06	146	0.09	0.05	190	0.12	0.25
10	0.00	0.00	56	0.05	0.13	102	0.29	0.40	147	0.05	0.04	191	0.08	0.14
11	0.39	0.00	57	0.57	1.35	103	0.28	0.53	148	0.05	0.02	192	0.07	0.16
12	0.14	1.34	58	1.03	0.90	104	0.03	0.16	149	0.08	0.06	193	0.80	0.05
15	0.14	0.00	59	0.08	0.53	105	0.27	0.41	150	0.05	0.09	194	0.12	0.55
16	0.00	0.00	60	2.62	2.09	106	0.06	0.19	151	0.03	0.03	195	0.11	0.07
17	0.00	0.00	61	1.56	0.37	107	0.19	0.37	152	0.02	0.07	196	0.34	0.28
18	1.58	0.00	62	0.45	0.09	108	0.34	0.72	153	0.10	0.02	197	0.15	0.45
19	0.74	0.19	63	0.37	0.04	109	1.45	1.48	154	0.25	0.16	198	0.38	0.45
20	0.52	1.11	64	1.95	0.60	110	0.52	1.44	155	0.54	0.27	199	0.67	0.25
21	0.07	0.31	65	3.01	0.26	111	0.17	0.98	156	0.12	0.71	200	0.29	0.15
22	1.21	0.47	66	0.00	0.10	112	0.52	0.00	157	0.73	0.00	201	0.05	0.00
23	0.41	1.30	67	0.35	0.93	113	0.33	0.15	158	2.18	1.61	202	0.67	0.95
24	0.40	0.07	68	0.57	0.24	114	0.06	0.44	159	0.65	0.84	203	0.24	0.61
25	0.33	0.44	69	0.67	0.20	115	1.30	0.73	160	0.52	0.26	204	0.07	0.43
26	0.10	0.43	70	0.43	0.25	116	1.01	0.25	161	0.08	0.20	205	0.24	0.09
27	0.06	0.92	71	0.21	0.27	117	0.42	0.28	162	0.10	0.17	206	0.01	0.15
28	0.20	0.65	72	0.12	0.44	118	0.33	0.07	163	0.10	0.06	207	0.03	0.31
29	0.12	0.55	73	0.14	0.42	119	0.02	1.08	164	0.43	0.74	208	0.06	0.05
30	0.90	0.00	74	0.08	0.13	120	0.38	0.02	165	0.25	0.78	209	0.06	0.24
31	0.91	0.92	75	0.15	0.18	121	0.96	0.45	166	0.04	0.39	210	0.05	0.30
32	0.57	0.84	76	0.03	0.14	122	0.09	0.09	167	0.57	0.00	211	0.10	0.01
33	1.19	0.26	77	0.59	0.39	123	0.26	0.69	168	0.09	0.19	212	0.16	0.14
34	1.14	0.62	78	0.19	0.04	124	0.13	0.04	169	0.05	0.00	213	0.21	0.07
35	0.48	1.02	79	0.02	0.44	125	0.14	0.05	170	0.13	0.21	214	0.01	0.12
36	0.78	1.08	80	0.79	0.12	126	0.01	0.07	171	0.50	0.13			
37	0.54	0.56	81	0.10	0.92	127	0.26	0.09	172	0.52	0.96			
38	0.56	0.49	82	0.41	0.22	128	0.01	0.00	173	0.62	1.62			
39	1.39	0.88	83	0.06	0.67	129	0.01	0.00	174	1.78	1.10			
40	0.38	0.81	84	0.00	1.49	130	0.09	0.22	175	2.33	1.46			
41	0.24	0.15	87	0.00	0.00	131	0.03	0.06	176	1.29	0.61			
42	0.71	0.11	88	0.00	0.00	132	0.12	0.33	177	0.32	0.00			
43	1.00	0.83	89	0.14	0.00	133	0.03	0.31	178	0.51	1.79			
44	0.07	0.26	90	2.14	1.00	134	0.43	1.17	179	0.38	0.03			
45	0.12	0.03	91	0.15	1.55	135	0.26	0.08	180	0.44	0.05			
46	0.08	0.11	92	0.03	0.36	136	0.27	0.25	181	0.12	0.14			
47	0.11	0.13	93	0.11	0.00	137	0.74	0.24	182	0.30	0.67			
48	0.82	0.60	94	0.50	0.17	138	0.49	0.10	183	0.56	0.29			

Table S5

Measured and back calculated values for residual dipolar couplings (RDCs) of $AdK^{cc,ox}$ (Hz). Back calculation was performed by AMP domain, ATP domain and core domain related residues (aa) of $AdK^{cc,ox}$ using the open-like apo wild type AdK structure 4AKE.pdb as well the closed-like Ap5a-bound AdK structure 1AKE.pdb.

aa^{AMP}	$RDC^{measure}$	RDC^{4AKE}	RDC^{1AKE}
30	3.5	-0.2	2.9
32	-5.7	-0.8	-5.4
35	-2.9	-3	-2.5
44	-5	-11.3	-2.4
48	-16	-11.9	-16.5
74	-9.9	-5.8	-11.7
77	3.2	1.3	2.3
78	2.5	5.2	0.4
79	-12.2	-11.7	-10.9

aa^{ATP}	$RDC^{measure}$	RDC^{4AKE}	RDC^{1AKE}
121	-7	-4.2	2.2
123	-9.4	5.8	-4.6
124	17.4	12.6	17
125	13.6	13.2	14.1
126	2.9	9.9	8.4
127	-5	-3.2	-5.7
129	-2.9	-3.9	-4.9
130	3.1	2.4	1.5
131	-10.9	-3.8	-6
132	10.1	12.2	12.9
134	14.4	4.6	8.2
135	5.9	10.4	7.7
136	-12.2	-8.5	-11.3
138	12.2	13.3	13.4
141	-0.5	-2.5	-1.3
142	-12.1	-3.5	-10.1
143	-10	-0.4	-5.5
144	-0.5	-5.7	-6.3
145	9.5	11.7	13.7
146	15.8	12.6	12.7
147	-12.2	-10.2	-14.4
148	-7.8	-6.1	-8.9
149	-12.2	-2.5	-6.5
150	-2.6	-0.5	-0.1
151	-9.6	1.8	-2.4
152	9.5	3.9	5.5
153	-8.4	-5.4	-6.8

aa^{ATP}	$RDC^{measure}$	RDC^{4AKE}	RDC^{1AKE}
154	-1.6	3	-1.6
155	7.3	12.8	7.3
156	17.4	13.9	17.4
157	3.6	0.9	3.6
159	-5.4	-1.6	-5.4

aa^{core}	$RDC^{measure}$	RDC^{4AKE}	RDC^{1AKE}
2	-1.2	-0.1	-3.8
3	-3.3	-1.5	-1.1
4	3.5	2.8	-2.5
6	20.2	12.1	20.3
18	-7.5	-14	-8.1
22	-17.3	-12.2	-12.1
28	-2.3	-5.6	-5.7
29	10.2	1.4	-2.1
80	8.9	4.2	13.4
81	-9.3	0.8	-3.4
82	-1.4	-2.2	-5.3
83	-0.5	-0.6	-1.2
84	5.1	0.4	-3.6
90	1.5	-7.2	-4.6
92	-19.1	-15.3	-15.3
93	-13.7	-8.5	-5.9
94	-9	-2.7	-5.5
95	-10.3	-13.8	-13.4
98	-11.3	-9.6	-6.9
99	-9.6	-16.3	-15.8
105	-1.5	1.6	2.1
106	-5.6	7.3	0.3
107	6.6	2.2	5.6
108	6.7	10.5	9.7
109	18.8	12.4	18.4
113	-2.2	-8.5	-7.6
114	-1.9	-3.8	-0.2
115	-13.3	-10.8	-13.2
116	-1.9	-7.5	-1.4
117	-0.9	-4.9	-7.2
118	-8.2	-3.7	-5.1

aa^{core}	$RDC^{measure}$	RDC^{4AKE}	RDC^{1AKE}
119	-16	-10.4	-6.4
120	-0.8	-3.4	-4.8
160	8.5	4.8	2.4
162	-12.8	-12	-8
163	-8	-12.6	-8.5
164	-9.6	-16.2	-13.2
165	-21.9	-15.9	-10.9
166	-14	-10.5	-9.9
179	-2	-4.6	-2.2
180	2.1	5.1	7.4
181	-1.6	-3.8	-5.4
182	-14.9	-8.6	-12.9
183	18.3	4.7	3.6
184	8.9	6.7	5.9
185	-4.5	-7.4	-5.8
186	-7.8	-6.4	-9.2
187	5.9	4.4	6.8
188	1.1	-1.5	-0.4

Table S6 Data collection and refinement statistics for complex formed between $AdK^{cc,ox}$ and Ap5a.

	$AdK^{cc,ox}$–Ap5a complex
Data collection	
Space group	$P2_122_1$
Cell dimensions	
a, *b*, *c* (Å)	73.00, 79.06, 81.83
α, β, γ (°)	90, 90, 90
Resolution (Å)	26.82–1.90 (1.97–1.90)*
R_{merge}	0.120 (1.99)
R_{pim}	0.033 (0.56)
$I/\sigma I$	18.8 (1.8)
Completeness (%)	99.6 (97.5)
Redundancy	14.6 (14.1)
Refinement	
Resolution (Å)	26.82–1.90 (1.97–1.90)
No. of reflections	37833 (3642)
R_{work}/R_{free}	18.6/23.6 (32.4.7/37.1)
No. of atoms	
Protein	3323
Ap5a	114
Co^{2+}	2
Water	552
B-factors (Å^2)	
Protein	35.6
Ap5a	25.2
Co^{2+}	28.4
Water	38.9

R.m.s. deviations	
Bond lengths (Å)	0.003
Bond angles (°)	1.16
Clashscore	1.0
Ramachandran plot (%)	
In preferred regions	99.0
In allowed regions	1.0
Outliers	0.0

*Values in parentheses are for the highest-resolution shell.

All data were collected from one crystal.

R.m.s., root mean square.

Table S7. Thermodynamic parameters and binding affinities of ATP, AMP and Ap5a interaction to wild type AdK, $AdK^{cc,ox}$, $AdK^{cc,red}$, AdK G56C and AdK T163C as probed by isothermal titration calorimetry at 25 °C.

AdK variant	**Ligand**	K_D **(μM)**	ΔH^0 **(kJ mol^{-1})**	$-T\Delta S^0$ **(kJ mol^{-1})**	***n***
Wild type	ATP	51±13[a]	−2.2±0.4[a]	−22.3[a]	1.0±0.1[a]
$AdK^{cc,ox}$	ATP	0.26±0.04	−70±2	33±2	0.50±0.01
$AdK^{cc,red}$	ATP	1.4±0.1	-3.1±0.5	-30.3±1.9	0.7±0.1
AdK G56C	ATP	2.7±1.0	-2.7±1.2	-29.2	0.7±0.1
AdK T163C	ATP	7.7±3.0	-6.3±2.0	-23.0	0.4±0.1
Wild type	AMP	210±70[b]	n.d.	n.d.	n.d.
$AdK^{cc,ox}$	AMP	1.2±0.1	−85±2	52±2	0.34±0.04
$AdK^{cc,red}$	AMP	n.d.	n.o.	n.d.	n.d.
AdK G56C	AMP	n.d.	n.o.	n.d.	n.d.
AdK T163C	AMP	n.d.	n.o.	n.d.	n.d.
AdK variant	**Ligand**	K_D **(nM)**	ΔH^0 **(kJ mol^{-1})**	$-T\Delta S^0$ **(kJ mol^{-1})**	***n***
Wild type	Ap5a	120±30[a]	-14.6±0.4[a]	-24.9[a]	0.45±0.01[a]
Wild type+TCEP	Ap5a	60±10	-14.6±0.4	-26.6	0.46±0.01
$AdK^{cc,ox}$ (site 1)	Ap5a	2.5±0.5	-80.9±0.4	31.8	0.44±0.01
$AdK^{cc,ox}$ (site 2)		250±50	-38.8±1.3	1.2	0.25±0.02
$AdK^{cc,red}$ (site 1)	Ap5a	10±3	-61.4±0.4	15.8	0.51±0.01
$AdK^{cc,red}$ (site 2)		650±50	-91.5±2.9	56.2	0.24±0.01
AdK G56C	Ap5a	140±20	-45.5±1.2	6.3	0.60±0.02
AdK T163C	Ap5a	160±20	-46.5±1.0	7.8	0.55±0.01

[a] From (16)

[b] From (17)

n.d., not determined.

n.o., not observable.

Supporting References

1. Kovermann M, et al. (2015) Structural basis for catalytically restrictive dynamics of a high-energy enzyme state. Nature Communications 6:7644.
2. Müller CW & Schulz GE (1992) Structure of the complex between adenylate kinase from Escherichia coli and the inhibitor Ap5A refined at 1.9 Å resolution. A model for a catalytic transition state. J. Mol. Biol. 224(1):159-177.
3. Kabsch W (2010) XDS. Acta Crystallogr. D Biol. Crystallogr. 66:125-132.
4. Winn MD, et al. (2011) Overview of the CCP4 suite and current developments. Acta Crystallogr. D Biol. Crystallogr. 67:235-242.
5. Adams PD, et al. (2010) PHENIX: a comprehensive Python-based system for macromolecular structure solution. Acta Crystallographica Section D 66(2):213-221.
6. Emsley P, Lohkamp B, Scott WG, & Cowtan KD (2010) Features and development of Coot. Acta Crystallogr. D Biol. Crystallogr. 66:486-501.
7. Krissinel E & Henrick K (2004) Secondary-structure matching (SSM), a new tool for fast protein structure alignment in three dimensions. Acta Crystallogr. D Biol. Crystallogr. 60:2256-2268.
8. Rhoads DG & Lowenstein JM (1968) Initial velocity and equilibrium kinetics of myokinase. J. Biol. Chem. 243(14):3963-3972.
9. Delaglio F, et al. (1995) NMRPipe: a multidimensional spectral processing system based on UNIX pipes. J. Biomol. NMR 6(3):277-293.
10. Johnson BA (2004) sing NMRView to visualize and analyze the NMR spectra of macromolecules. Methods Mol. Biol. 278:313-352.
11. Salzmann M, Wider G, Pervushin K, & Wüthrich K (1999) Improved sensitivity and coherence selection for [15N,1H]-TROSY elements in triple resonance experiments. J. Biomol. NMR 15:181-184.
12. Farrow NA, et al. (1994) Backbone dynamics of a free and a phosphopeptide-complexed Src homology-2 domain studied by N-15 NMR relaxation. Biochemistry 33(19):5984-6003.
13. Dosset P, Hus JC, Marion D, & Blackledge M (2001) A novel interactive tool for rigid-body modeling of multi-domain macromolecules using residual dipolar couplings. J. Biomol. NMR 20:223-231.
14. Loria JP, Rance M, & Palmer AG (1999) A relaxation-compensated Carr-Purcell-Meiboom-Gill sequence for charactherizing chemical exchange by NMR spectroscopy. J. Am. Chem. Soc. 121:2331-2332.
15. Jenik M, et al. (2012) Protein frustratometer: a tool to localize energetic frustration in protein molecules. Nucl. Acid. Res. 40:348-351.
16. Olsson U & Wolf-Watz M (2010) Overlap between folding and functional energy landscapes for adenylate kinase conformational change. Nature Communications 1:111.
17. Ådén J, Verma A, Schug A, & Wolf-Watz M (2012) Modulation of a Pre-existing Conformational Equilibrium Tunes Adenylate Kinase Activity. Journal of the American Chemical Society 134:16562-16570.